

# ADVERSARIAL PAIRWISE REVERSE ATTENTION FOR CAMERA PERFORMANCE IMBALANCE IN PERSON RE-IDENTIFICATION: NEW DATASET AND METRICS

Eugene P.W. Ang<sup>†\*</sup> Shan Lin<sup>†\*</sup> Rahul Ahuja<sup>‡</sup> Nemath Ahmed<sup>§</sup> Alex C. Kot<sup>\*</sup>

<sup>\*</sup>Rapid-Rich Object Search (ROSE) Lab, Nanyang Technological University, Singapore

<sup>‡</sup>Computer Science Department, New York University, New York, USA

<sup>§</sup>Department of Electrical Engineering, Indian Institute Technology Indore, Indore, India

## ABSTRACT

Existing evaluation metrics for Person Re-Identification (Person ReID) models focus on system-wide performance. However, our studies reveal weaknesses due to the uneven data distributions among cameras and different camera properties that expose the ReID system to exploitation. In this work, we raise the long-ignored ReID problem of camera performance imbalance and collect a real-world privacy-aware dataset from 38 cameras to assist the study of the imbalance issue. We propose new metrics to quantify camera performance imbalance and further propose the **Adversarial Pairwise Reverse Attention (APRA)** Module to guide the model towards learning camera invariant features with a novel pairwise attention inversion mechanism.

**Index Terms**— Person Re-identification, Data Imbalance, Adversarial Learning, Attention

## 1. INTRODUCTION

Person re-identification, also known as Person ReID, deals with matching images or videos of the same person over a multiple-camera surveillance system. Although it enjoys rapid progress, issues remain during the transition to real-world deployment. For example, the standard metrics applied on a per-camera basis reveal that certain cameras in the network systematically under-perform their peers. Such vulnerabilities open the system up to exploitation by adversaries determined to evade it.

In order to quantify the performance imbalance of different cameras, we propose two new metrics for camera-specific evaluation: (1) camera query mean Average Precision (mAP) and (2) camera gallery mAP, which we shorten to **query-mAP** and **gallery-mAP** respectively. The query-mAP reports the performance when all query images are from one specific camera. On the other hand, the gallery-mAP measures the ease of retrieving positives from a particular camera. Figure 1 (a) and (c) show the camera-level Person ReID performance of a baseline model trained on the Market-1501 [1] and

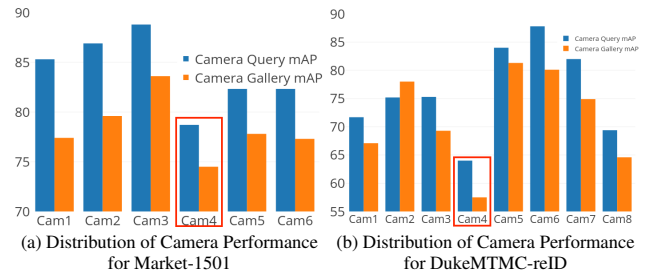


**Fig. 1.** Camera Performance Imbalance Problem in Market-1501 and DukeMTMC-reID, outlined in red.

DukeMTMC-reID [2] datasets. Cameras 4 in both Market-1501 and DukeMTMC-reID datasets, outlined in red, lower the overall performance of the system.

Our proposed **Adversarial Pairwise Reversed Attention (APRA)** module leverages a novel pairwise attention inversion mechanism to disentangle camera features from identity features, utilizing adversarial gradient reversal to further suppress camera information. Adding our module to state-of-the-art methods better balances inter-camera performance on all four benchmarks studied in this paper.

To summarize, our contributions are as follows: (i) We identify and quantify inter-camera performance imbalance by formulating new per-camera metrics. (ii) We contribute a large-scale outdoor ReID dataset, NTU-Outdoor-38, boasting more cameras than other ReID datasets. (iii) We propose APRA, a module based on our novel paired attention inversion mechanism and apply it to state-of-the-art models to demonstrate better performance balance among cameras.

## 2. RELATED WORK

Modern Person ReID methods are mostly based on deep convolutional neural networks. Early deep learning based work usually formulated Person ReID as a verification problem and as a result solutions developed were based on Siamese architectures [3, 4, 5]. In recent years, verification-driven approaches such as [6, 7] evolved from two-stream Siamese structures to triplet architectures to add robustness to the ver-

<sup>†</sup>Equal contribution.

ification system. Another dominant approach is to formulate the Person ReID problem as a classification task. Zheng *et al.*[8] first proposed the ID-discriminative embedding (IDE) to train an image to person ID mapping using models pre-trained on ImageNet [9]. Sun *et al.*[10] optimized the fully connected (FC) feature corresponding to person IDs with Singular Vector Decomposition (SVD). Many recent approaches [11, 12, 13] consist of both classification loss and verification loss. The latest approaches, such as HA-CNN [14], AANet [15] and DuATM [16], utilize attention mechanisms to further boost the Person Re-ID performance.

Few studies have considered camera-level features and per-camera performance evaluation. Zhong *et al.*[17] first discovered that image style variations caused by different cameras affect ReID retrieval results. They proposed a new data augmentation technique, CamStyle, which uses a CycleGAN [18] to generate new training images by combining appearance features from one camera and camera-style features from another camera. Zhang *et al.*[19] and Zhu *et al.*[20] train Person ReID models specialized on individual cameras. Unlike our study, the main motivation behind their work is to reduce ReID annotation labor by restricting the annotator’s scope to a single camera.

### 3. NTU-OUTDOOR DATASET

#### 3.1. Overview of Previous Datasets

Compared to real-world video surveillance systems that keep track of hundreds of cameras, existing Person ReID datasets such as Market-1501 [1], DukeMTMC-reID [2] and MSMT17 [21] contain a limited number (6-15) of cameras. This is primarily because annotation difficulty increases with the number of cameras, limiting its scalability. Additionally, most existing ReID datasets capture subjects without their awareness and consent. This lack of curation has raised privacy concerns from the public.

#### 3.2. Privacy-Aware Data Collection

To address privacy/consent concerns, we apply a new privacy-aware data collection strategy during the collection of our new dataset. We developed a mobile application with functions for participants to declare consent, log their own appearance attributes, upload a reference picture of themselves and record their location over the duration of the data collection exercise to narrow the annotation window. We only annotate images belonging to consenting participants and discard images of other pedestrians.

#### 3.3. Dataset Characteristics

Figure 2 provides some sample images from Market-1501 [1], DukeMTMC-reID [2], MSMT17 [21], and also our NTU-Outdoor-38 dataset. Market-1501 and MSMT17 used non-surveillance cameras, resulting in an unrealistic near-horizontal point of view of subjects.



**Fig. 2.** Comparison of images in Market-1501, DukeMTMC-reID, MSMT17 and NTU-Outdoor-38.

Dataset	NTU-Outdoor-38	MSMT17	DukeMTMC-reID	Market-1501
# Cameras	<b>38</b>	15	8	6
# Images	48,347	<b>126,441</b>	36,411	32,668
# Identities	549	<b>4,101</b>	1,812	1,501
Privacy	<b>Signed Agreement</b>	-	-	-
Camera Type	<b>Surveillance</b>	Normal	<b>Surveillance</b>	Normal
Detector	YOLO V3	Faster RCNN	DPM	DPM
Attribute	<b>40</b>	-	23	30

**Table 1.** Comparison between NTU-Outdoor-38 and other Person ReID datasets

In the NTU-Outdoor-38 dataset, images are captured from actual surveillance cameras mounted on lamp-posts, better highlighting the viewing angles and imbalances inherent in real-world networked camera systems. It consists of outdoor scenes with large changes in viewpoint, illumination, and resolution that manifest even within individual wide-angle cameras. Our dataset spans 38 cameras, significantly more than other popular benchmarks. There are 549 appearance identities with signed privacy agreements for using their images for academic purposes. The NTU-Outdoor-38 dataset also comes with 40 additional binary attributes annotated by participants. Table 1 presents the characteristics of the NTU-Outdoor-38 dataset compared against Market-1501 [1], DukeMTMC-reID [2] and MSMT17 [21]. NTU-Outdoor-38 captures the inter-camera performance imbalances present in real-life camera networks and serves as an excellent test-bed to further study this problem. To the best of our knowledge, it is the only publicly available Person ReID dataset collected from over 30 cameras.

### 4. CAMERA-LEVEL EVALUATION METRICS

We present two new per-camera metrics to evaluate the performance of individual cameras in a ReID system. Query

mAP (q-mAP) is a grouping of the query set by disjoint camera ids:  $\text{mAP}_c^q = \frac{1}{|Q_c|} \sum_{q \in Q_c} \text{AP}(q, G)$ , where  $Q_c$  is the set of query images captured from Camera  $c$ ,  $G$  is the gallery set and AP is the average precision metric.

Conversely, Gallery mAP (g-mAP) keeps only the positives from a chosen camera during retrieval, ignoring other positive candidates from other cameras. This helps us to evaluate the ease of retrieving positive gallery candidates from a chosen camera only. The g-mAP of Camera  $c$  is given as  $\text{mAP}_c^g = \frac{1}{|Q_c|} \sum_{q \in Q_c} \text{AP}(q, G_q)$ , where  $G_q$  is the gallery set excluding other positives not captured by Camera  $c$  and  $Q_c$  is the set of queries that have at least one positive in the gallery from Camera  $c$ .

## 5. PROPOSED METHOD

### 5.1. APRA Module

Figure 3 illustrates the architecture of our APRA module. The APRA module is comprised of two key pieces: **Pairwise Reverse Attention** and **Adversarial Gradient Reversal**. First, it introduces a new camera classification branch. The input feature is dynamically divided into different branches via reversed pairwise attention, and we apply adversarial gradient reversal on the camera branch to encourage learning of camera-invariant ID features. Our modules can be placed in between layers of a standard deep convolutional neural network. Based on our experiments, placing the APRA module in early layers yields the best performance.

#### 5.1.1. Pairwise Reverse Attention

Our APRA module, as shown in Figure 3 divides an input feature map between person and camera classification branches. This division is negotiated using attention mechanisms that operate on the channel and spatial dimensions of the feature map. Figure 3 visualizes one example of our learned in spatial attention maps. Our proposed module operates similar to a “foreground” and “background” separation where it naturally teaches the model to focus on the subject for id classification and on the surroundings for camera classification. Our APRA module performs the same disentanglement along the channel dimension, which is harder to visualize.

Given a feature map  $\mathbf{F} \in \mathbb{R}^{C \times H \times W}$ , we follow [22] to derive a  $\mathbb{R}^{C \times 1 \times 1}$  channel attention tensor  $M_c$  and a  $\mathbb{R}^{1 \times H \times W}$  spatial attention tensor  $M_s$ . We extend this technique by deriving an inverse channel attention  $M'_c = 1 - M_c$  and an inverse spatial attention  $M'_s = 1 - M_s$ . The input to the person branch is given by  $\mathbf{F}_\rho = [(\mathbf{F} \otimes M_c) \otimes M_s + \mathbf{F}]_+$ , where  $\otimes$  is element-wise multiplication with broadcasting. Conversely, the camera branch output is derived from the reverse attention maps  $\mathbf{F}_\kappa = [(\mathbf{F} \otimes M'_c) \otimes M'_s + \mathbf{F}]_+$ . Thus, our APRA module exploits reverse attention to generate a separate feature pathway for the camera classification branch.

Division of input features induces competition between both pathways, but can also be symbiotic: higher-level se-

mantic features are suitable for person identification, whereas lower-level style-based features suit camera classification. By placing APRA among earlier layers of the base model (Figure 3), we foster cooperation; low-level camera features are purged upstream, allowing the model to focus on learning id-relevant high-level features, reducing the tendency to over-fit and thus balancing performance between cameras.

#### 5.1.2. Adversarial Gradient Reversal

Drawing inspiration from [23], during back-propagation we reverse the gradients by multiplying all gradients up to the camera output branch of the APRA module (Figure 3) by a negative scalar. This adversarial setup encourages the model to learn camera-invariant features by reducing the tendency to over-fit to cameras.

### 5.2. Combined Loss Function

The first loss function we use is cross entropy,  $\mathcal{L}_{CE} = -\frac{1}{n} \sum_{i=1}^n \log(p_\theta(y_i|x_i))$ , where  $x_i$  are the training images,  $y_i$  are the corresponding (either person or camera identity) ground-truth labels,  $n$  is the number of samples in the batch and  $\theta$  are the model parameters. The second loss function is the triplet loss,  $\mathcal{L}_{triplet} = \frac{1}{|T|} \sum_{a,p,n \in T} [\delta_\theta(a,p) - \delta_\theta(a,n) + m]_+$ , where  $T$  is the set of triplets,  $\delta$  is a distance metric and  $m$  is a positive margin. The person identity loss is  $\mathcal{L}_\rho = \mathcal{L}_{CE}^{Person} + \mathcal{L}_{triplet}$ . The camera identity loss is  $\mathcal{L}_\kappa = \mathcal{L}_{CE}^{Camera}$ . Our proposed solution is a combination of both branch losses,  $\mathcal{L} = \mathcal{L}_\rho + \lambda \mathcal{L}_\kappa$ . In all our experiments, the hyperparameter  $\lambda = 0.01$ . Once the model is trained, we use the embeddings from the person branch.

## 6. EXPERIMENTS

### 6.1. Dataset and Setting

We perform comparisons over three of the most popular benchmarks: Market-1501 [1], DukeMTMC-reID [2], MSMT17 [21] and our NTU-Outdoor-38 dataset, which we abbreviate to Market, Duke, MSMT and NTU-38 respectively. The statistics of each dataset are reported in Table 1. Each dataset gets more challenging as the number of cameras increases. For system-wide performance evaluation, we adopt the widely used Rank-1 and mAP scores. For detailed camera level evaluation, we use our newly proposed query-mAP and gallery-mAP.

### 6.2. Performance Evaluation

#### 6.2.1. Camera Performance Evaluation

We evaluate our method’s improvement in camera-specific performance on Market, Duke, MSMT and NTU-38, using Q-mAP and G-mAP to denote query-mAP and gallery-mAP, respectively. As shown in Table 2, the weakest cameras reap the most improvements in all benchmarks, achieving more substantial gains compared to other cameras. Also, datasets



## 8. ACKNOWLEDGEMENTS

This work was supported by the Defence Science and Technology Agency (DSTA). It was carried out at the Rapid-Rich Object Search (ROSE) Lab at the Nanyang Technological University, Singapore.

## 9. REFERENCES

- [1] Zheng et al, "Scalable Person Re-identification: A Benchmark," in *ICCV*, 2015.
- [2] Zheng et al, "Unlabeled Samples Generated by GAN Improve the Person Re-identification Baseline in Vitro," in *ICCV*, 2017.
- [3] Wang et al, "Joint Learning of Single-Image and Cross-Image Representations for Person Re-identification," in *CVPR*, 2016.
- [4] Huang et al, "Multi-Pseudo Regularized Label for Generated Data in Person Re-Identification," *TIP*, 2019.
- [5] Lin et al, "End-to-End Correspondence and Relationship Learning of Mid-Level Deep Features for Person Re-Identification," in *DICTA*, 2017.
- [6] Hermans et al, "In Defense of the Triplet Loss for Person Re-Identification," in *arXiv preprint*, 2017.
- [7] Chen et al, "Beyond Triplet Loss: A Deep Quadruplet Network for Person Re-identification," in *CVPR*, 2017.
- [8] Zheng et al, "Person Re-identification: Past, Present and Future," *arXiv preprint*, 2016.
- [9] Deng et al, "ImageNet: A large-scale hierarchical image database," in *CVPR*, 2009.
- [10] Sun et al, "SVDNet for Pedestrian Retrieval," in *ICCV*, 2017.
- [11] Paisitkriangkrai et al, "Learning to rank in person re-identification with metric ensembles," in *CVPR*, 2015.
- [12] Wang et al, "Learning Discriminative Features with Multiple Granularities for Person Re-Identification," in *ACM MM*, 2018.
- [13] Luo et al, "Bag of Tricks and a Strong Baseline for Deep Person Re-Identification," in *CVPRW*, 2019.
- [14] Li et al, "Harmonious Attention Network for Person Re-identification," in *CVPR*, 2018.
- [15] Tay et al, "AANet: Attribute Attention Network for Person Re-Identifications," in *CVPR*, 2019.
- [16] Si et al, "Dual Attention Matching Network for Context-Aware Feature Sequence Based Person Re-identification," in *CVPR*, 2018.
- [17] Zhong et al, "Camera Style Adaptation for Person Re-identification," in *CVPR*, 2018.
- [18] Zhu et al, "Unpaired Image-to-Image Translation Using Cycle-Consistent Adversarial Networks," *ICCV*, 2017.
- [19] Zhang et al, "Single Camera Training for Person Re-Identification," in *AAAI*, 2020.
- [20] Zhu et al, "Intra-camera supervised person re-identification: A new benchmark," in *ICCVW*, 2019.
- [21] Wei et al, "Person Transfer GAN to Bridge Domain Gap for Person Re-identification," in *CVPR*, 2018.
- [22] Woo et al, "CBAM: Convolutional block attention module," in *ECCV*, 2018.
- [23] Ganin et al, "Domain-Adversarial Training of Neural Networks," *JMLR*, 2016.
- [24] Song et al, "Mask-Guided Contrastive Attention Model for Person Re-identification," in *CVPR*, 2018.
- [25] Qi et al, "A Mask Based Deep Ranking Neural Network for Person Retrieval," in *ICME*, 2019.
- [26] Kalayeh et al, "Human Semantic Parsing for Person Re-identification," in *CVPR*, 2018.
- [27] Wang et al, "Mancs: A Multi-task Attentional Network with Curriculum Sampling for Person Re-Identification," in *ECCV*, 2018.
- [28] Qian et al, "Pose-normalized image generation for person re-identification," in *ECCV*, 2018.
- [29] Zhizheng Zhang, Cuiling Lan, Wenjun Zeng, Xin Jin, and Zhibo Chen, "Relation-aware global attention for person re-identification," *CVPR*, 2020.